

Contents

1	Design & Simulation	1
1.1	Design Requirements	1
1.2	Design overview	2
1.3	Optical Design of the OCT Beampath	3
1.3.1	Fourier Plane Scanner	3
1.3.2	Component Selection	5
1.3.3	Minimization of backreflections	6
1.3.4	Single Modality Probe	7
1.3.5	Optical Performance	7
1.4	Mechanical Design	8
1.4.1	Resonant frequency calculation	9
1.4.2	COMSOL simulation	10
2	Fabrication and Assembly	13
2.1	Polyimide Electrodes	14
2.1.1	Cleanroom processing	15
2.2	Fiber-GRIN Bonding	16
2.3	3D Printed Housing	17
2.4	Assembly	18

Contents

Nomenclature

Latin letters

variable	meaning	unit
A	area	m^2
w	width	m
c	concentration	wt.%
d	diameter	m
G	Gibbs free enthalpy	J
h	height	m
l	length	m
m	mass	kg
p	pressure	Pa
r	radius	m
Re	Reynolds-number	
t	time	s
V	volume	m^3

Greek letters

variable	meaning	unit
α	absorption coefficient	$1/\text{m}$
γ	surface tension	N/m
η	dynamic viscosity	Ns/m^2
θ	contact angle	$^\circ$, rad
κ	curvature	$1/\text{m}$
λ	wave length	m
ν	kinematic viscosity	m^2/s
ρ	specific gravity	kg/m^3

Indices

Nomenclature

index	meaning
<i>lg</i>	liquid-gas
<i>sg</i>	solid-gas
<i>sl</i>	solid-liquid
<i>la</i>	liquid-ambient

Abbreviations

abbreviation	meaning
2D	2-dimensional
AF	amorphous fluoropolymer
DFR	dry film resist
DI	deionized ultra-pure water
DRIE	Deep reactive ion etching
ICP	Inductive coupled plasma
MEMS	Micro-electro-mechanical system
PDMS	Polydimethylsiloxan
PEB	Post Exposure Bake
PMMA	Polymethylmethacrylat
UV-Vis	ultraviolet to visible wavelengths

1 Design & Simulation

The aim of this work is to design and test a miniaturized OCT microscope as a component of a multi-modal endoscope. As described in Chapter ??, this probe consist of two spectrally-separated optical paths that run partially in parallel through a micro-optical bench system. This approach allows independent tuning of the optical parameters of the two imaging modalities – such as the NA or depth of field – while still providing a geometrical overlap of the two acquired images. An integrated tubular piezoelectric fiber scanner is used to perform en face scanning required for three dimensional OCT measurements. This scanning engine has an outer diameter of 0.9 mm and a length of 9 mm, and features custom fabricated 10 μm thick polyimide flexible interconnect lines to address the four piezoelectric electrodes.

The following section describes the conception and design of the endoscope, starting from the medical and geometrical requirements, through analytical modeling and towards the optimization of each component.

1.1 Design Requirements

The OCT microscope should fulfill the following requirements:

Mechanical Requirements

- The scanner, electrical connections and optics should fit in a 1 mm \times 1 mm square channel located in the lower level of the multimodal bench (total cross section 3.05 \times 2 mm²). Its length should be minimized.
- The field of view should be maximized for a 2 mm diameter objective lens, which is shared with the endomicroscopy beampath.
- The scanning speed should be adequate for the sampling rates characteristic of SD-OCT (\sim 100 kHz).

Optical Requirements

- The microscopy and OCT imaging fields should be coaxial to avoid parallax errors.
- The OCT field should be distal-side telecentric to avoid field curvature distortions and to maximize the collection of backscattered light upon normal incidence to the tissue.

1 Design & Simulation

- The lateral resolution and depth of field should be adequate for OCT, with numerical apertures ranging from 0.02 to 0.05.
- The backreflections inside the probe should be minimized to avoid

1.2 Design overview

The main challenge of this work is to design a scanning mechanism compact enough to be placed in a thin, buried channel of a multimodal probe. Although it is theoretically possible to keep a scanner at the proximal end of the endoscope and use a coherent fiber bundle (CFB) as a relay, there are inherent drawbacks of this method, such as low light throughput, cross-talk and mechanical rigidity [?].

Another challenging requirement is the superposition of the images acquired by the different modalities. If the optical axes are not coaxial, the fields will be shifted and tilted due to parallax error — which gains importance at the small working distances common in endoscopy.

To overcome these problems, and taking into account the above-mentioned requirements, we propose a design comprising a resonant fiber scanner followed by a beam splitter (BS), illustrated in Figure 1.1, as an evolution of the HYAZINT multimodal probe [?], using a two layer microbench to combine white light microscopy and 3D OCT.

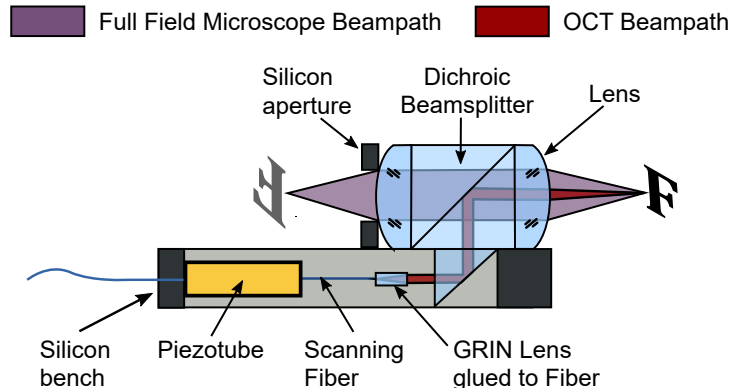


Figure 1.1: Schematic of the MEMS endomicroscope. Two glass lenses glued directly to the dichroic beamsplitter cube form the full field microscopy beam path. A silicon aperture is used to reduce the spherical aberrations. Buried beneath the full field optics, a single mode fiber glued to a collimating GRIN lens forms the OCT channel. The single-mode fiber is fixed in a piezoelectric tube to create a fiber scanner enabling 3D OCT. A reflecting micro-prism glued to a dichroic beamsplitter cube combines the two beampaths.

The base of the microbench with dimensions of 13 x 2 x 1mm³ is realized by standard silicon bulk micromachining. On the top layer, the bench accommodates

the full field imaging optics that consists of a dichroic beamsplitter cube with dimensions of $2 \times 2 \times 2\text{mm}^3$ to separate the two beam paths and two plano-convex lenses with 2mm diameter, which form the full field microscope. To achieve a highly compact opto-mechanical design, the components of the OCT beam path are buried within a cavity in the base of the micro bench. On the bottom layer a gradient index lens (GRIN lens) with a diameter of 350 um is directly glued to the tip of a 80 um single mode fiber to collimate the infrared light of the OCT system with a center wavelength of $\lambda_0 = 1.31 \text{ um}$ and a bandwidth of $\Delta\lambda = 90 \text{ nm}$. A spiral scanning of the OCT beam path is achieved by an angular scanner implemented using a piezoelectric tube actuator.

This actuator, called resonant fiber scanner, is able to scan a collimated beam more than $\pm 5^\circ$ by mechanically amplifying the subtle vibration of a piezoelectric actuator. An objective lens then focuses the beam on the tissue and transforms the angular displacement into translation. By driving the scanner in two axes with two sinusoids, it is possible to sample a 2D area of the object in a spiral fashion, as explained in detail in section ??.

The rest of this chapter shows the design and development of the OCT imaging path for the multi-modal probe. However, in order to independently test the behavior of the OCT scanner and optics, a single modality probe was fabricated as a demonstrator. Both systems are mechanically and optically equivalent – the only difference is the presence of the beam splitter.

For completeness, both multi-mode and single-mode optical systems are described.

1.3 Optical Design of the OCT Beampath

This section explains in detail the design of the OCT optics and its scanning mechanism. Starting with the concept of Fourier plane scanner, the most relevant design equations are derived, which guide the selection of the optical components to achieve the desired performance, eventually verified by optical simulation.

Furthermore, the sources of backreflections in the probe are analyzed and minimized.

1.3.1 Fourier Plane Scanner

The OCT beam path is designed as an object-sided telecentric system to avoid distortions in the 3D OCT measurement. To achieve this, the fiber scanner is driven with small angles and is positioned such that the lateral and angular movement of the scanner imitates the beam angles that can be observed in the collimated region of a classical telecentric lens system. Figure 1.2 illustrates this approach. The whole scanner will be buried in a channel with a inner diameter of 1 mm limiting the movement of the scanner to a maximum angle θ of 5° that allows a maximum FOV of 1 mm of the OCT beam path.

1 Design & Simulation

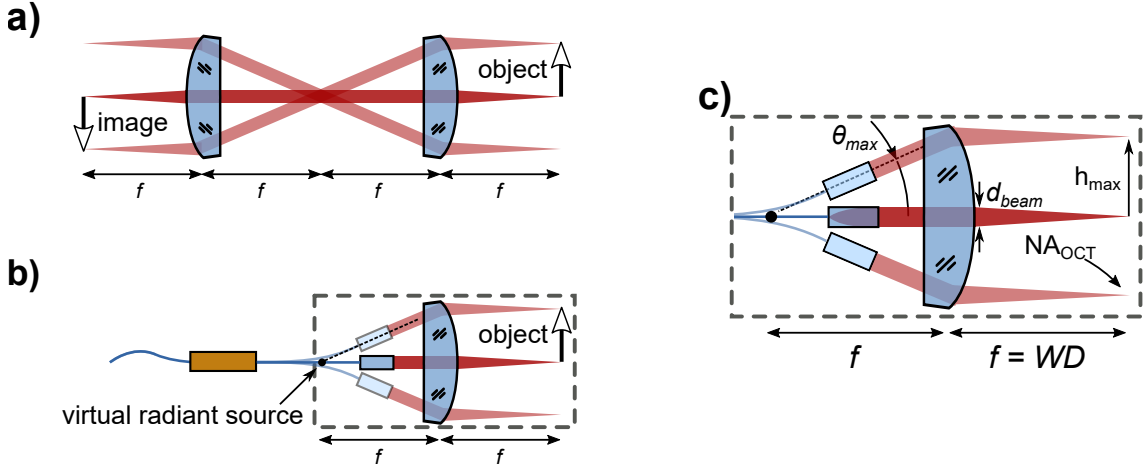


Figure 1.2: **a)** Illustration of a classical telecentric system. The height of the object is translated into an angle θ in the collimated region between the two lenses. This angle is again translated into a corresponding image height by the second lens. **b)** Illustration of the OCT beam path using a fiber scanner in first resonance mode without micro prism and BS. The movement of the GRIN lens due to the fiber scanner and the distance between the GRIN lens and the focusing lens creating the same optical behavior as it can be observed in a classical object sided telecentric system. **c)** Nomenclature used in this work.

For the scanner to work as a Fourier plane scanner, at any point of the oscillation the output beam from the GRIN lens should point to a fixed virtual radiant source. This is fulfilled if the bending shape of the scanner is linear with the amplitude and thus, the ratio of the GRIN lens angle to its vertical displacement is kept constant $y = d \cdot \tan \theta \simeq d \cdot \theta \Rightarrow \frac{\theta}{y} = const$ (refer to Figure 1.3).

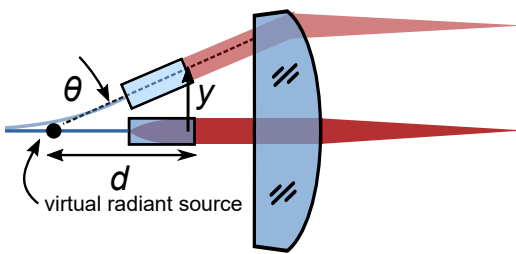


Figure 1.3: Schematic of the Fourier plane scanner at rest and at an arbitrary position with amplitude θ . If the scanner behaves linearly, the output beam will appear to come from a fixed virtual radiant source regardless of the scanning amplitude.

1.3.2 Component Selection

In a Fourier plane scanner, the numerical apertures and focal lengths of the scanning and objective lens are related by the diameter of the beam in the intermediate region between both lenses. Thus, following the schematic of Figure 1.2c, we can obtain the following geometrical optics relations: $d_{\text{beam}} \simeq 2 \cdot f_{\text{GRIN}} \cdot NA_{\text{fiber}}$ and $d_{\text{beam}} \simeq 2 \cdot f_{\text{obj}} \cdot NA_{\text{OCT}}$. By combining them together we arrive to the main design equation for the scanner:

$$f_{\text{GRIN}} \cdot NA_{\text{fiber}} = f_{\text{obj}} \cdot NA_{\text{OCT}} \quad (1.1)$$

Note that these equations use a small angle approximation valid for small NA: $\tan[\sin^{-1}(NA)] \simeq NA$. For example, if NA = 0.2, the error of this simplification is smaller than 2%.

The design of the optical path for OCT is constrained by the commercial availability of the components. In this case, the only single mode fiber working in our wavelength range and with thinned cladding diameter (refer to Section 1.4) is *Thorlabs SM980G80*, with a diameter of 80 μm and with $NA_{\text{fiber}} = 0.18$ at 1.330 μm .

In order to collimate the output from the fiber without clipping the gaussian beam we need a GRIN lens with an NA_{GRIN} higher than NA_{fiber} . A good fit from GRINTECH catalog is *GT-LFRL-035-024-20-CC (1550)*, with an $NA_{\text{GRIN}} = 0.20$ and $f_{\text{GRIN}} = 0.91 \text{ mm}$.

Now, by using the relation in Equation ?? we can design $f_{\text{objective}}$ by choosing an adequate NA_{OCT} . To preserve a high depth of field (DOF), allow enough space for the beamsplitter and a long working distance, a narrow NA_{OCT} is preferred – in the range of 0.020 - 0.025. By choosing an intermediate NA_{OCT} of 0.022, the focal length of the objective lens $f_{\text{obj}} = f_{\text{GRIN}} NA_{\text{fiber}} / NA_{\text{OCT}} = 0.91 \text{ mm} \cdot 0.18 / 0.022 = 7.5 \text{ mm}$ can be selected.

The field of view (FOV) of the OCT modality can be now calculated considering the maximum angular deflection of the GRIN lens in the tip of the scanning fiber by $h_{\text{max}} = f_{\text{obj}} \cdot \tan \theta_{\text{max}} = 7.5 \text{ mm} \cdot \tan 5^\circ = 0.66 \text{ mm}$, equivalent to a FOV of 1.2 mm for a θ_{max} of $\pm 5^\circ$ (section 1.4).

ZEMAX Simulation

In order to validate the theoretical analysis of the optical design, we proceeded to a raytracing simulation using ZEMAX. By modeling the fiber facet as the waist of a gaussian beam, using the GRIN lens model provided by the manufacturer and a geometrical model of the prism, beamsplitter and planoconvex lens, we obtain the schematic shown in Figure 1.4a.

The three overlapping rectangles on the left simulate the rest position (red) and maximum deflection (purple) of the GRIN lens. The gap between GRIN lens and prism is numerically optimized for telecentricity and maximum FOV.

Due to the low NA_{OCT} and the good optical quality of the GRIN and planoconvex lenses, we achieve diffraction-limited imaging, as seen in the spot diagrams through

1 Design & Simulation

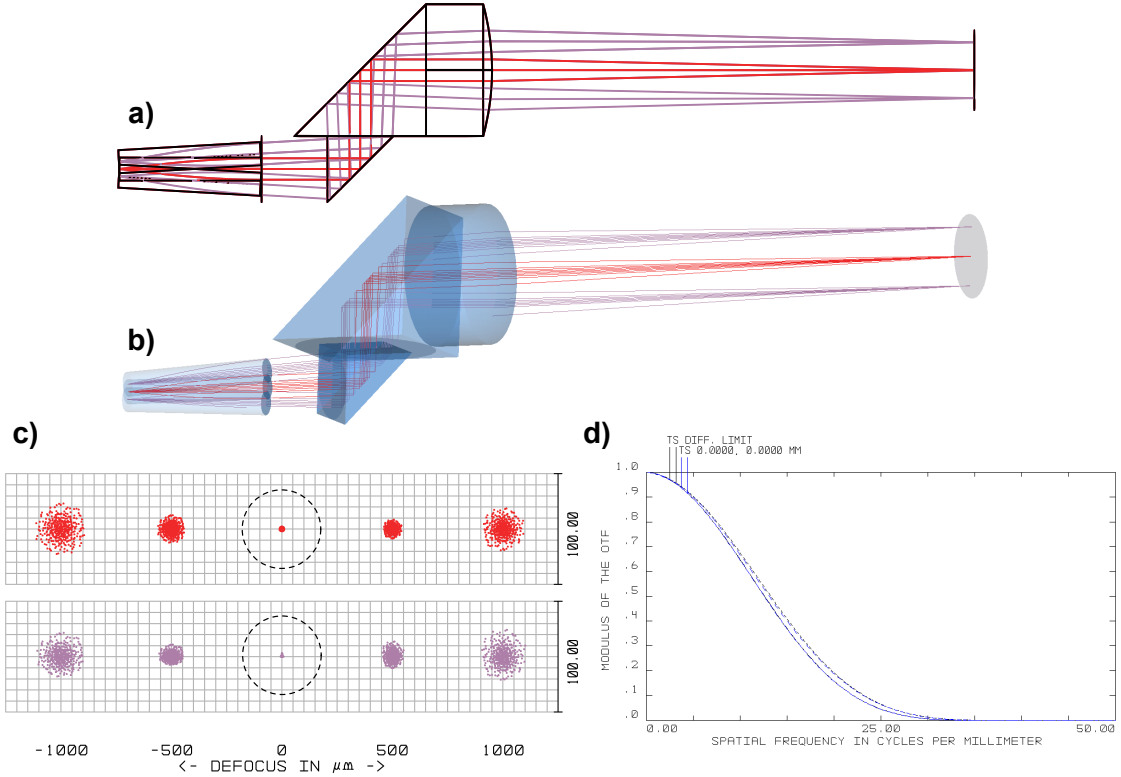


Figure 1.4: **a)** ZEMAX schematic of the OCT beampath for the center (red) and maximum (purple) position of the GRIN lens. **b)** 3D representation. **c)** Spot diagram through focus for center (red) and marginal (purple) rays, showing the Airy circle. Dimensions in μm . **d)** MTF of the system for Tangential and Sagittal directions.

focus (Figure 1.4c) and the MTF curve (Figure 1.4d).

1.3.3 Minimization of backreflections

In Fourier Domain OCT, any backreflection coming from the probe increases the background intensity and therefore reduces the penetration depth and contrast of the resultant image. Thus any source of backreflections in the design should be carefully considered and minimized:

- **Fiber-GRIN Interface:** Starting from the proximal side, the fiber-GRIN interface consists of two parallel glass surfaces separated by a small gap. Although the beam is not collimated in this region, a small portion of light can be coupled back to the fiber. In order to minimize any backreflections, fiber and GRIN are glued together using a refractive-index-matched optical adhesive (*NOA 76*, from *Norland Products*). This way there is no glass to air interface and the maximum refractive index step is reduced to 0.05.

- **GRIN-Air Interface:** The next interface is the distal facet of the GRIN lens. This is the most critical interface – regardless of the scanning angle, it exhibits normal, collimated light incidence. To avoid this problem without resorting to delicate and expensive antireflection coatings (ARC), the GRIN lens is manufactured with a 1° tilted exit facet. According to geometrical optics, this tilt induces a vertical shift in the position of the backreflected focal point given by equation 1.2:

$$\Delta y = f \tan(2\alpha) = 0.91 \text{ mm} \cdot \tan(2^\circ) = 31 \mu\text{m} \quad (1.2)$$

The result is visible in the simulation from Figure 1.5: the backreflected light is focused back with a $31 \mu\text{m}$ offset, therefore missing the core of the fiber – which has a diameter inferior to $5 \mu\text{m}$.

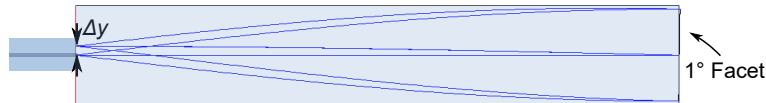


Figure 1.5: Simulation of backreflected light upon the distal end of a GRIN lens with a 1° tilted facet.

- **Air-Prism Interface:** Due to collimated incidence, this interface exhibits can produce backreflections, but only in a single position of the GRIN lens – where both facets are parallel. An ARC would be nevertheless beneficial.
- **Objective Lens - Air Interface:** After the prism, the beamsplitter and objective lens are cemented together, making any backreflections negligible. The objective lens has an interface with air, but due to the curved surface, the light won't be coupled back in a significantly. Nevertheless, the distal surface of the lens are ARC.

1.3.4 Single Modality Probe

As stated in the Design Overview, in order to independently test the behavior of the OCT scanner and optics, a single modality probe was fabricated as a demonstrator. Both systems are mechanically and optically equivalent – the only difference is the presence of the beam splitter. Figure 1.6 shows the ZEMAX simulation of this configuration, where the parallelism with the multimodal probe can be seen.

1.3.5 Optical Performance

Table 1.1 summarizes the theoretical and simulated optical performance of the OCT microscope in both single modality of multimodality configurations.

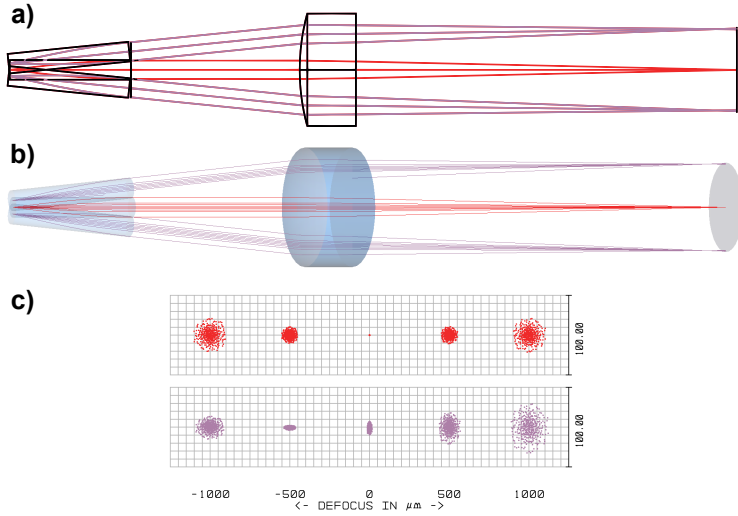


Figure 1.6: **a)** ZEMAX schematic of the single modality probe for the center (red) and maximum (purple) position of the GRIN lens. **b)** 3D representation. **c)** Spot diagram through focus for center (red) and marginal (purple) rays, showing the Airy circle. Dimensions in μm .

Distal Side NA	0.022
Working Distance	7.3 mm
Field of View	1.2 mm
Depth of Field	3.4 mm
Lateral Resolution	43 μm

Table 1.1: Simulated optical performance and characteristics of OCT modality. All resolution values follow the Rayleigh convention.

1.4 Mechanical Design

The fiber scanner uses resonance to amplify the subtle movement of the piezoelectric tube (in the order of $\pm 3 \mu\text{m}$) into a big displacement and angular deflection of the GRIN lens (in the order of $\pm 350 \mu\text{m}$ and $\pm 5^\circ$). Therefore, its geometrical and mechanical characteristics fully define the operating frequency range, and with it, constrain the way we can sample and acquire the final image.

As a resonant system, the movement of the scanning fiber is constrained to harmonic oscillations with a frequency close to $f_{resonance}$. Thus, the number of sample points N_T that can be acquired in period T depend on the resonant frequency of the scanner and the sampling frequency of the OCT system:

$$N_T = \frac{f_{sampling}}{f_{resonance}} \quad (1.3)$$

As OCT systems have a relatively small sampling frequency ($\pm 100 \text{ kHz}$), we need

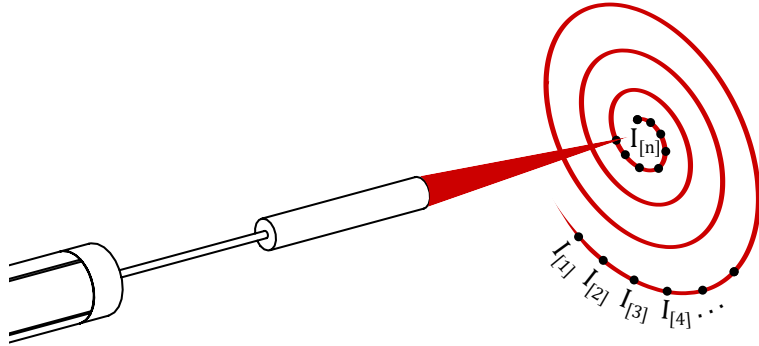


Figure 1.7: Movement of the laser spot through time (red) and acquired points (black) during spiral scanning.

to decrease the resonant frequency below 1 kHz to achieve more than 100 points per sampling period. The following paragraphs describe how to calculate and reduce this frequency.

1.4.1 Resonant frequency calculation

Following Euler Bernoulli theory, the spring constant for a fixed-free, point loaded cantilever is given by Equation 1.4, considering that the moment of inertia of the cylindrical fiber is given by $I_{fiber} = \frac{\pi}{4}r^4$.

$$K_{cantilever} = \frac{3EI}{L^3} = \frac{3\pi}{4} \frac{E_{fiber} r_{fiber}^4}{L^3} \quad (1.4)$$

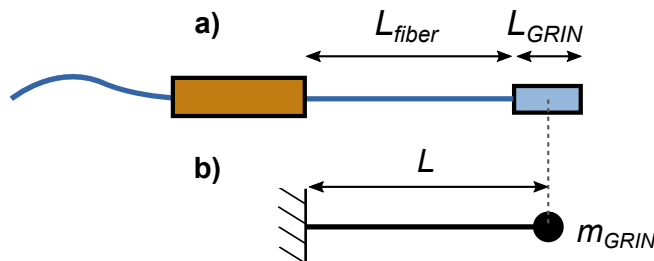


Figure 1.8: **a)** Drawing of the piezoelectricscanner: piezoelectric tube, fiber and GRIN lens. **b)** Simplified mechanical diagram,

Approximating the fiber - GRIN assembly as a weightless, flexible, fixed-free cantilever and concentrating the weight of the GRIN lens in its center of gravity (Figure 1.8), we can estimate the resonant frequency of the scanner by applying the ideal mass-spring harmonic resonator equation for the first resonant mode (Eq. 1.5)¹.

¹In order to assess the error of this approximation, we repeated the calculation of the resonant frequency using the method described in [?]. In the plotted range, the error was smaller than 2%.

1 Design & Simulation

$$f_{res} = \frac{1}{2\pi} \sqrt{\frac{K_{cantilever}}{m_{GRIN}}} \quad (1.5)$$

As we can observe from equation 1.4 and 1.5, the resonance frequency increases quadratically with the diameter of the fiber. Therefore, by choosing a fiber with 80 μm instead of the standard 125 μm , the resonance frequency can be lowered from 1900 Hz to 770 Hz for a 4.5 mm scanner.

The resonant frequency of a cantilever formed by a 80 μm fused silica fiber with the chosen GRIN lens is computed in Figure 1.9.

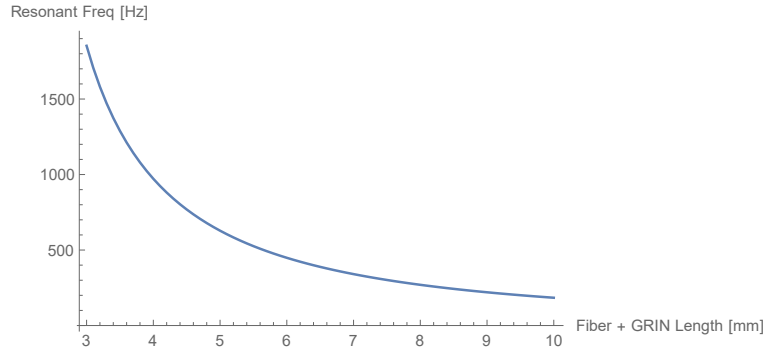


Figure 1.9: Resonant frequency as a function of the scanning tip length (fiber + GRIN lens).

As the scanner is buried in a 1 mm channel, the maximum displacement of the GRIN lens is limited to $\pm 325 \mu\text{m}$. Within that small displacement we want to achieve the maximum angular deflection of the GRIN lens to maximize the FOV, what can be achieved by using shorter fiber lengths. This shows a trade-off with the density of sampling N_T – which is increased with longer fiber lengths. To balance those terms, we chose a total scanner length of 4.5 mm, with characteristics summarized in Table 1.2.

Total scanner length	4.5 mm
Resonant Frequency	770 Hz
Max. angular deflection	5°

Table 1.2: Mechanical characteristics.

1.4.2 COMSOL simulation

In order to validate the theoretical analysis of the previous section, we performed a multiphysics FEM analysis using COMSOL. For that matter, the piezoelectric actuator was modeled as a radially polarized piezoelectric material (*PIC 151*) and

the rest of the structure as elastic material. The excitation voltage is a sinusoidal symmetrical potential between the top and bottom electrodes of the tube. As the system undergoes small deflections, it is simulated assuming linear behavior [?].

The first step is to simulate the resonant frequency of the system. Performing an *Eigenfrequency* study, we obtain a first mode resonance at 762 Hz, which closely matches our analytical estimation (770 Hz. The mode shape is shown in Figure 1.10.

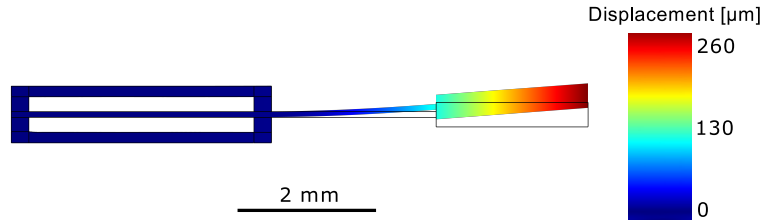


Figure 1.10: COMSOL simulation of the total deflection in at resonance (762 Hz).

Note that, as the system is working at its resonance, it is very difficult to simulate the oscillation amplitude, as it depends on its damping factor which should be obtained experimentally. Thus, for the simulation, this value was chosen to fit the expected deflection.

Thanks to the multiphysics simulation, we can also check the electric field distribution inside the piezoelectric tube. As can be seen in Figure 1.11, for a symmetrical actuation in the left and right electrodes with a voltage of ± 75 V, most of the volume under those electrodes experiences a field magnitude close to the expected theoretical value $E = U/d = 75 \text{ V}/150 \mu\text{m} = 500 \text{ V/m}$, which is under the safe operating field of *PIC 151*: $+1000 \text{ V/m}$ to -700 V/m . Only some fringe areas exceed these values, which could become depolarized with time.

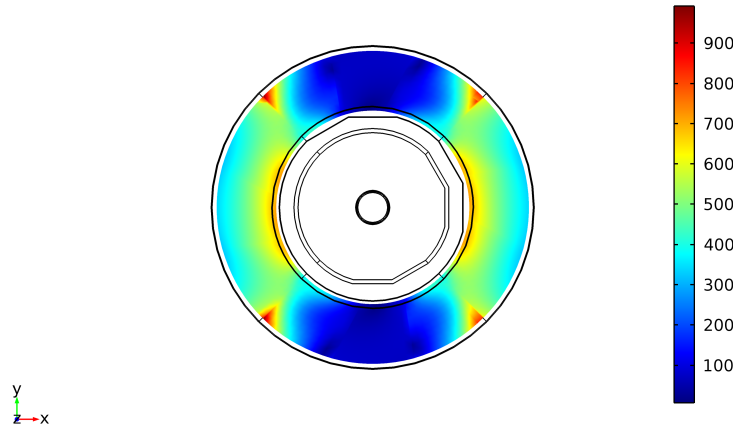


Figure 1.11: Magnitude of the electrical field [kV/m] inside a cross-section of the piezoelectric tube with an excitation voltage of ± 75 V

1 Design & Simulation

2 Fabrication and Assembly

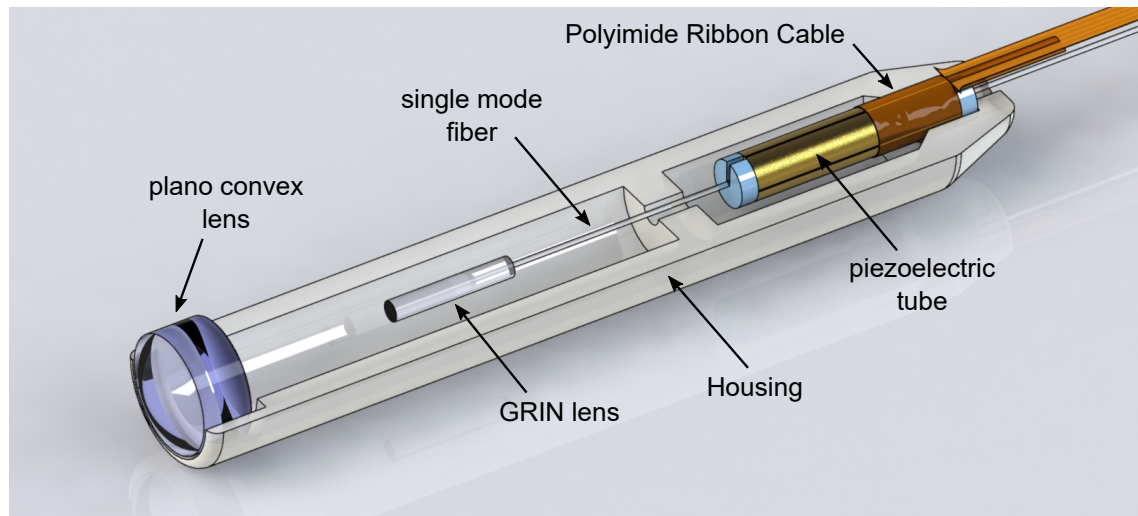


Figure 2.1: CAD of the single modality demonstrator with the top of the housing removed. Total length: 9 mm.

The probe shown in Figure 2.1 was built as a demonstrator of the fiber scanner design and evaluation of the optical performance of the OCT beam path.

The piezoelectric actuator with four outer gold electrodes to control the lateral movement of the scanner is supplied by PI Ceramic. The addressing of these electrodes is realized by a polyimide-based ribbon cable, which is wrapped around the piezoelectric tube. Conductive glue is applied through via holes in the ribbon cable to enable the connection between the platinum from the conductors and the gold pads of the piezotube surface. The single mode fiber is centered in the piezoelectric tube using small FR-2 discs and the GRIN lens bonded to the tip of this fiber using optical adhesive.

This arrangement enables a compact fiber scanner with a total length of 9 mm and a resonance frequency of 750 Hz optimized for an OCT system with an A-Scan repetition rate of 100 kHz.

The following paragraphs describe the manufacturing process of the most relevant components of the probe.

2.1 Polyimide Electrodes

Due to the small diameter of the piezoactuator, contacting its electrodes reliably is not trivial. Other piezosscanner implementations use soft soldering and insulated copper wires [?], [?], [?]. The soldering process can damage the actuator, as it is exposed to temperatures above its Curie temperature. This method also increases significantly the diameter of the actuator, as a solder blob is needed. Furthermore, it requires welding by hand in a 600 µm curved electrode – certainly not production-friendly.

Instead, we developed a polyimide ribbon cable which is wrapped around the piezotube and addresses its 4 external electrodes with vias. Its geometry, cross section and rolled state are depicted in Figure 2.2.

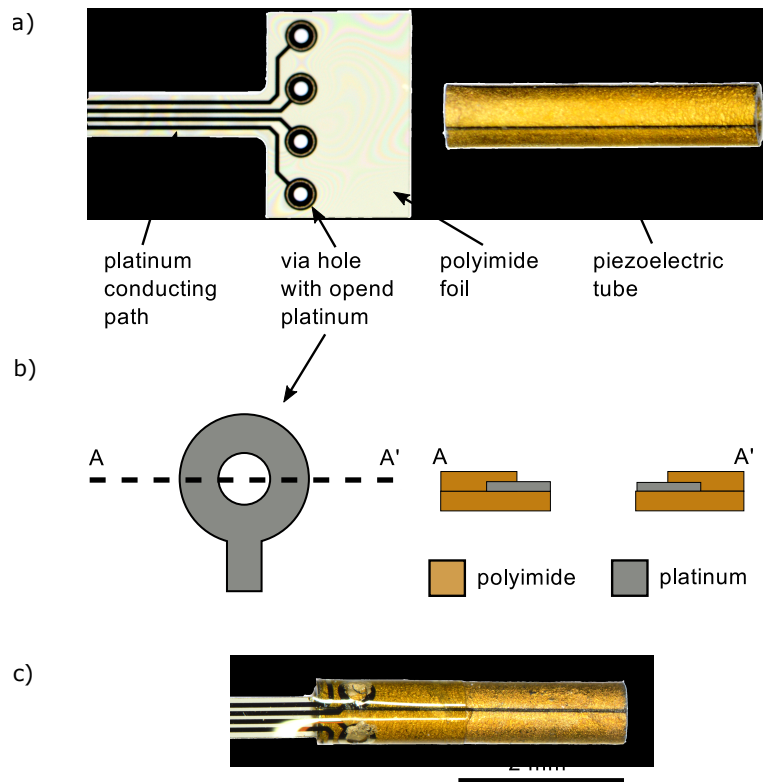


Figure 2.2: **a)** Left: Photo of the polyimide ribbon cable with four vias to contact the four gold electrodes of the piezoelectric tube. Right: Piezotube. **b)** Schematic of one via and its cross section. The platinum around the via is partly uncovered to improve the electrical connection between the cable and the piezoelectric tube. **c)** Photo of a polyimide ribbon cable, wrapped around the piezoelectric tube that is electrical connected through the vias by conductive glue.

It is manufactured using a cleanroom process similar to the one used for cuff electrodes for nerve stimulation [?] and consists of platinum tracks and via holes

embedded in a polyimide substrate. One end the cable is shaped to fit a zero insertion force (ZIF) connector. The other end can be rolled around the piezotube, allowing the bonding to its gold electrodes using conductive glue (Araldite 2020 with 80% wt. silver particles).

2.1.1 Cleanroom processing

The polyimide ribbon cables are manufactured and singulated at wafer level. The process involves spincoating a 5 μm layer of polyimide, over which 100 nm of platinum is sputtered and then patterned by liftoff, defining the conductive traces. Finally, the vias, openings and external shape are patterned through reactive ion etching (RIE). This process is described in Figure 2.3.

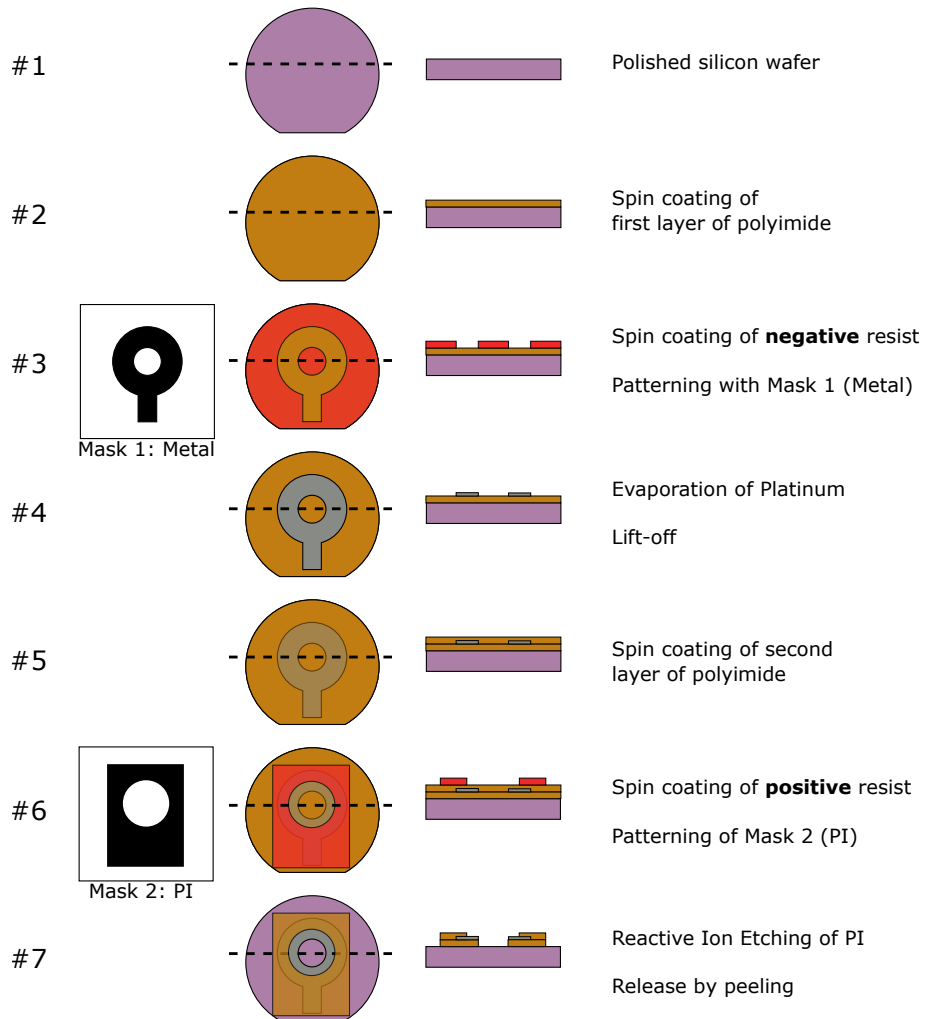


Figure 2.3: Cleanroom fabrication process of the polyimide electrodes.

2.2 Fiber-GRIN Bonding

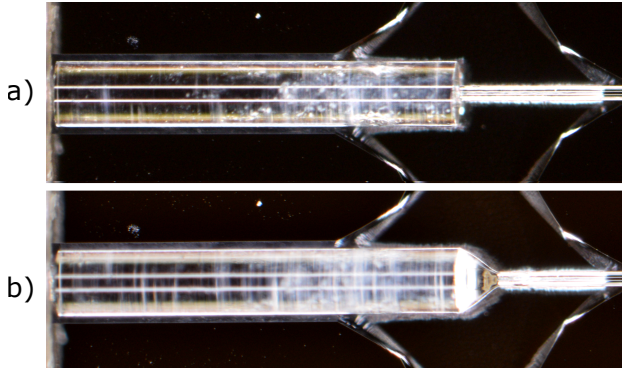


Figure 2.4: Fiber and GRIN lens in silicon alignment tool before (a) and after (b) bonding with UV-curable adhesive.

The GRIN lens and the end of the fiber have to be bonded together mechanically and optically for the proper functioning of the probe. This interface is critical: first, because it is subjected to very high forces due to the oscillation of the scanner, and second, because any angular or displacement error would degrade the optical quality.

To overcome these challenges, we align the fiber to the GRIN lens using a custom made, KOH-etched silicon alignment tool. The precise geometry of the KOH-etched grooves allow a very good angle and position control of the cylindrical fiber and GRIN lens. Once in place, we apply a drop of optical UV-curable glue (NOA 76), which thanks to its wetting behavior and surface tension, creates a symmetrical wedge which provides extra mechanical integrity.

figures/foo.png

Figure 2.5: Cross section with dimensions

2.3 3D Printed Housing

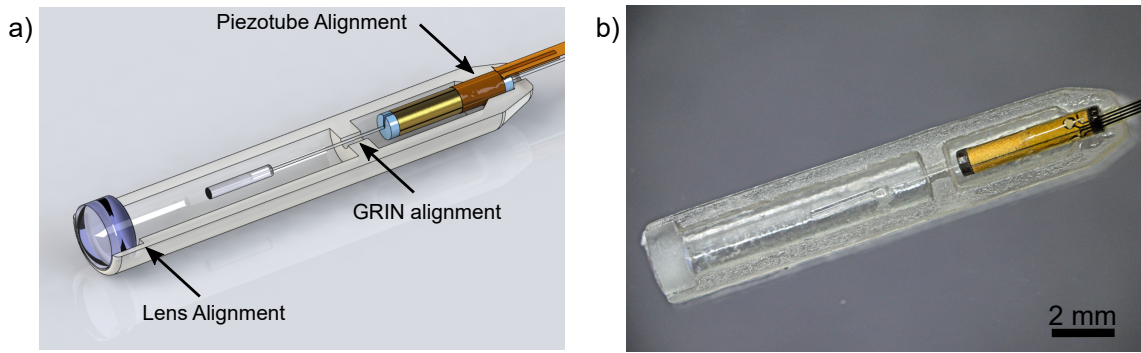


Figure 2.6: CAD (a) and photography (b) of the single modality probe with alignment features.

Although the bimodal probe is designed to be assembled using the silicon bench technology, we assembled the demonstrator in a 3D printed plastic housing, with no degradation in its optical quality. This is possible because the most critical alignment – fiber to GRIN – is performed beforehand. The rest of the components allow relatively high placement tolerances, as the beam is collimated in the region between GRIN lens and objective lens. This way, simple alignment structures which are 3D-printed in the housing allow the proper placement of all the components.

(Material, printer, process?)

For example, in order to center the piezotube in the housing, first the fiber is retracted so that the GRIN lens seats in the GRIN alignment structure (Figure 2.7 left). This way the piezotube is aligned in the housing and, after being glued in place, it is possible to push the fiber so that the GRIN is at its proper distance (Figure 2.7 right).

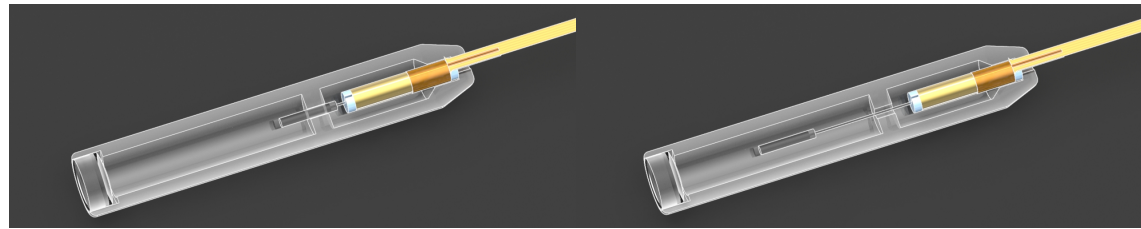


Figure 2.7: Alignment of the piezotube-fiber-GRIN assembly in the housing.

2.4 Assembly



Figure 2.8: Exploded view of the components of the single modality probe.

The assembly process is summarized as follows:

1. The GRIN lens is bonded to the end of the fiber.
2. The GRIN-fiber assembly is slid through the piezotube and centered with FR-2 fittings, which are glued to the piezotube using cyanocrylate.
3. The piezotube-fiber-GRIN assembly is placed in the housing and glued in place using cyanocrylate with help of the alignment structures.
4. The planoconvex lens is placed in the bottom half of the housing and glued using UV-curable optical glue.
5. The probe is closed with the top half of the housing and sealed with UV-curable glue.

Note of Thanks

Lastly, I wish to express my gratitude to those many people, who helped me in the last six months, for their contribution to success of this Master Thesis.

I want to thank Prof. Hans Zappe and my second corrector Prof...

Thanks to our group leader Chuck Norris.

Thanks to my supervisor.

Finally I want to thank my family, my friends and my dog.